Computers & Structures Vol. 47, No. 4/5, pp. 871–891, 1993
Printed in Great Britain.

0045-7949/93 $6.00 + 0.00
Pergamon Press Ltd

AN ARBITRARY LAGRANGIAN–EULERIAN VELOCITY POTENTIAL FORMULATION FOR FLUID–STRUCTURE INTERACTION

C. NITIKITPAIBOON and K. J. BATHE
Massachusetts Institute of Technology, Cambridge, MA 02139, U.S.A.

Abstract—Finite element formulations for fluid–structure interaction, assuming an inviscid fluid, can be classified into two major categories: displacement-based formulations and potential-based formulations. Although displacement-based formulations have been used widely, the methods suffer from the presence of spurious circulation modes and locking behavior. Potential-based formulations are inherently irrotational and do not have the difficulties of the displacement-based formulations. Nevertheless most of the applications of these methods are still limited to cases with relatively small motions. We introduce in this paper an arbitrary Lagrangian–Eulerian formulation using the velocity potential and the density as fluid variables. The formulation can be applied to problems in which the fluid undergoes very large boundary motions and can be used equally well for both compressible and incompressible fluids.

1. INTRODUCTION

The interaction between fluids and structures can, in many practical engineering problems, significantly affect the response of the structure and hence needs to be properly taken into account in the analysis. An inviscid-compressible fluid model (acoustic fluid model) often suffices for the application and is typically used in the analysis and design of nuclear reactor components, liquid-filled tanks, ships, and marine structures. As a result, a number of finite element formulations have been proposed to model the acoustic fluid for the analysis of fluid–structure interaction problems. These formulations may be classified into two major categories, namely, the displacement-based formulations and the potential-based formulations.

In the first category, the displacement-based formulations, the fluid motion is described by finite element nodal displacements. The fluid and the structure are coupled by equating the normal displacement component along the boundary common to the fluid and the structure. The equilibrium on the interface is then automatically enforced through the element assemblage process. This type of formulation is similar in structure to the displacement formulation generally used to model solids and, in its original form, can be thought of as the displacement formulation for an elastic solid with a negligible shear modulus [1]. Although the method has been used with success in a great deal of applications it was noted by many researchers that the pure displacement formulation for an inviscid fluid exhibits spurious circulation modes. Various approaches were introduced to obtain improved formulations [2–4], however, the formulations still fall short of being efficient and reliable.

In the second category, the fluid motion is represented by some form of scalar potential function. The use of potential functions instead of displacements makes the formulations in this category inherently free from spurious circulation modes. Both the compatibility condition and the equilibrium condition on the interface must be explicitly enforced. The formulations belonging to this category are the pressure formulation, the displacement potential formulation, the velocity potential formulation, the velocity potential and density formulation, and the displacement potential and pressure formulation. The majority of the work in this category of formulations is only applicable to linear problems.

The pressure formulation [5] and the displacement potential formulation are both nonsymmetric formulations and thus undesirable from a computational point of view. The displacement potential–pressure formulation, introduced by Morand and Ohayon [6, 7], employs both the displacement potential and the pressure as fluid unknown variables. Although the formulation leads to symmetric matrices, twice the number of degrees of freedom compared with the pure pressure formulation are required.

The use of the velocity potential formulation for fluid–structure problems was first suggested by Everstine [8]. Olson and Bathe [9] extended the formulation by including a uniform hydrostatic pressure in the formulation in order to eliminate the rigid body mode and enable the solution of static problems. The formulation yields a symmetric banded system of equations with only one variable per nodal point and therefore represents a very appealing approach. The coupling between the fluid and the solid is provided through the coupling matrix involving time derivatives of the fluid velocity potential and the solid displacements. As a result, some special considerations are required in solving the corresponding quadratic eigenproblem.

More recently, a Eulerian form of the nonlinear velocity potential–density formulation was introduced by Kock and Olson [10]. Although the method is useful in a variety of problems, its application is still limited to cases with relatively small boundary displacements. One simple approach to address this limitation is to use a mesh reconstruction scheme separately to allow larger boundary movements. Alternatively, and more rigorously, we can employ an arbitrary Lagrangian–Eulerian (ALE) description, which accurately takes into account the non-Eulerian nature of the finite element mesh with the moving boundary and in which both the Lagrangian and the Eulerian formulations are embedded. Mesh updating is an integral part of the formulation when using the ALE description.

We present in this paper a fully nonlinear velocity potential–density formulation based on the ALE approach for fluid–structure interaction. In the following sections, first the linear form of the velocity potential–density formulation is given. Then we discuss and summarize the theory of the arbitrary Lagrangian–Eulerian description. Next the ALE form of the proposed formulation is presented in detail. Finally, numerical examples are provided to demonstrate the capability of the formulation.

1.1. *Velocity potential–density formulation*

Considering an irrotational and isentropic inviscid fluid in small displacements without gravity effects as in [9], the governing equations can be written as

$$\frac{c_0^2}{\rho_0}\rho_1 + \dot{\phi} - \lambda = 0, \quad \text{in } \mathscr{R}_0 \tag{1}$$

$$\dot{\rho}_1 + \rho_0 \operatorname{div}(\operatorname{grad}\phi) = 0, \quad \text{in } \mathscr{R}_0 \tag{2}$$

$$\int_{\mathscr{R}_0} \rho_1 \, dV_0 - \int_{\partial\mathscr{R}_0} \rho_0 u_n \, dA_0 = 0 \tag{3}$$

$$\frac{\partial\phi}{\partial n} = 0, \quad \text{on } \partial\mathscr{R}_0^E \tag{4}$$

$$\frac{\partial\phi}{\partial n} = \dot{u}_n, \quad \text{on } \partial\mathscr{R}_0^M \tag{5}$$

$$\rho_0(\dot{\phi} - \lambda) = -\bar{p}, \quad \text{on } \partial\mathscr{R}_0^M, \tag{6}$$

where ϕ is the velocity potential, ρ_0 is the initial density, ρ_1 is the change in the density, λ is the unsteady Bernoulli constant, c_0 is the initial sound wave speed, $\mathscr{R}_0$ is the fluid domain, $\partial\mathscr{R}_0^E$ is the fixed part of the fluid boundary, $\partial\mathscr{R}_0^M$ is the part of the boundary corresponding to a free surface or a fluid–structure interface, $\dot{u}_n$ is the positive inward normal velocity of the boundary $\partial\mathscr{R}_0^M$, and $\bar{p}$ is the pressure prescribed on $\partial\mathscr{R}_0^M$. We note that eqns (1) and (2) are the linear form of the Bernoulli equation and the continuity equation, respectively, and eqn (3) is the global mass conservation equation.

The weak forms corresponding to eqns (1)–(6) are [11]

$$\int_{\mathscr{R}_0} \delta\rho \left(\frac{c_0^2}{\rho_0}\rho_1 + \dot{\phi} - \lambda\right) dV_0 = 0 \tag{7}$$

$$\int_{\mathscr{R}_0} (\delta\phi\dot{\rho}_1 - \rho_0 \operatorname{grad}\phi \cdot \operatorname{grad}\delta\phi)\, dV_0 - \int_{\partial\mathscr{R}_0} \rho_0 \delta\phi \dot{u}_n \, dA_0 = 0 \tag{8}$$

$$\delta\lambda \int_{\mathscr{R}_0} \rho_1 \, dV_0 - \delta\lambda \int_{\partial\mathscr{R}_0} \rho_0 u_n \, dA_0 = 0 \tag{9}$$

$$\int_{\partial\mathscr{R}_0} \delta u_n \rho_0 (\dot{\phi} - \lambda) \, dA_0 + \int_{\partial\mathscr{R}_0} \delta u_n \bar{p} \, dA_0 = 0. \tag{10}$$

After discretization, we obtain

$$\begin{bmatrix} \mathbf{0} & \mathbf{C}_{\rho\phi} & \mathbf{0} & \mathbf{0} \\ -\mathbf{C}_{\rho\phi}^T & \mathbf{0} & \mathbf{0} & \mathbf{C}_{\phi u^B} \\ \mathbf{0} & \mathbf{0} & \mathbf{0} & \mathbf{0} \\ \mathbf{0} & -\mathbf{C}_{\phi u^B}^T & \mathbf{0} & \mathbf{0} \end{bmatrix} \begin{bmatrix} \dot{\boldsymbol{\rho}} \\ \dot{\boldsymbol{\phi}} \\ \dot{\lambda} \\ \dot{\mathbf{U}}^B \end{bmatrix} + \begin{bmatrix} \mathbf{K}_{\rho\rho} & \mathbf{0} & \mathbf{K}_{\rho\lambda} & \mathbf{0} \\ \mathbf{0} & \mathbf{K}_{\phi\phi} & \mathbf{0} & \mathbf{0} \\ \mathbf{K}_{\rho\lambda}^T & \mathbf{0} & \mathbf{0} & \mathbf{K}_{\lambda u^B} \\ \mathbf{0} & \mathbf{0} & \mathbf{K}_{\lambda u^B}^T & \mathbf{0} \end{bmatrix} \begin{bmatrix} \boldsymbol{\rho} \\ \boldsymbol{\Phi} \\ \lambda \\ \mathbf{U}^B \end{bmatrix} = \begin{bmatrix} \mathbf{0} \\ \mathbf{0} \\ \mathbf{0} \\ \mathbf{R}_{u^B} \end{bmatrix}, \tag{11}$$

where the submatrices are evaluated from the corresponding integrals

$$\mathbf{K}_{\rho\rho}: \int_{\mathscr{R}_0} \delta\rho \frac{c_0^2}{\rho_0}\rho_1 \, dV_0 \qquad \mathbf{C}_{\rho\phi}: \int_{\mathscr{R}_0} \delta\rho\dot{\phi} \, dV_0$$

$$\mathbf{K}_{\rho\lambda}: -\int_{\mathscr{R}_0} \delta\rho\lambda \, dV_0 \qquad \mathbf{C}_{\phi u^B}: \int_{\partial\mathscr{R}_0^M} \delta\phi\rho_0\dot{u}_n \, dA_0$$

$$\mathbf{K}_{\phi\phi}: \int_{\mathscr{R}_0} \rho_0 \operatorname{grad}\delta\phi \cdot \operatorname{grad}\phi \, dV_0$$

$$\mathbf{R}_{u^B}: \int_{\partial\mathscr{R}_0^M} \delta u_n \bar{p} \, dA_0$$

$$\mathbf{K}_{\lambda u^B}: \int_{\partial\mathscr{R}_0^M} \delta\lambda\rho_0 u_n \, dA_0 \tag{12}$$

and the vectors $\boldsymbol{\rho}$, $\boldsymbol{\Phi}$, and $\mathbf{U}^B$ contain the nodal variables. The scalar value of λ pertains to the complete fluid domain. In this formulation the Bernoulli equation and the continuity equation are separately enforced. As a result the corresponding matrix equations do not involve the second-order time derivative or the 'mass' matrix but extra degrees

of freedom are required for ρ. Associated with the kinetic energy and the internal energy of the fluid are submatrices $\mathbf{K}_{\phi\phi}$ and $\mathbf{K}_{\rho\rho}$, respectively. The matrix $\mathbf{C}$ and the remaining parts of $\mathbf{K}$ join the two parts of the fluid's energy and couple the flexible (structure) interface to the fluid. We can represent an incompressible fluid by using only the velocity potential and the normal boundary displacement as variables and we can analyze static problems by discarding all terms involving the velocity potential from the above equations.

Letting $\delta\rho$ be equal to $\delta\phi$ and substituting for $\lambda = P_0/\rho_0$ we can eliminate ρ_1 from the above set of equations to obtain the same set of governing equations as employed by Olson and Bathe [9] for the velocity potential formulation. After discretization, the equivalence of the two formulations, the velocity potential (U–ϕ–P_0) formulation and the velocity potential–density (U–ϕ–ρ–λ) formulation, will still hold provided that we choose the space for ρ and $\delta\rho$ to be the same as that for ϕ and $\delta\phi$, that is, provided we choose the same shape functions for ρ and ϕ. Of course, in analyzing linear problems, the U–ϕ–ρ–λ formulation is, with twice the number of degrees of freedom per fluid node, not as efficient as the U–ϕ–P_0 formulation and therefore is of limited practical use. The benefits of introducing the density arise when considering nonlinear behavior.

Before we proceed to give the details of the new ALE velocity potential–density formulation we first summarize the theoretical concept of the arbitrary Lagrangian–Eulerian description in the next section.

2. VELOCITY POTENTIAL–DENSITY ALE FORMULATION

2.1. *Preliminaries*

In analyzing continuum mechanics problems, two types of descriptions are used, namely, the Lagrangian description and the Eulerian description. In the Lagrangian description, commonly used in solid mechanics, we refer to a quantity of interest by associating its value with a material particle identified via the particle's location in the initial configuration. On the other hand, in the Eulerian description we associate the quantity of interest with a point in the domain without regard to any specific material particle. This description is widely used in fluid mechanics.

In finite element analysis we describe any state variable through the mesh. A Lagrangian finite element mesh therefore represents the deformation of the material body, i.e., the motion of the mesh coincides with the particle motion. In contrast, a Eulerian finite element mesh is fixed in space. The arbitrary Lagrangian–Eulerian (ALE) formulation is a more general formulation that embeds the two descriptions mentioned above. In this formulation, the mesh is allowed to move but the motion of a mesh point does not necessarily coincide with the motion of a particle.

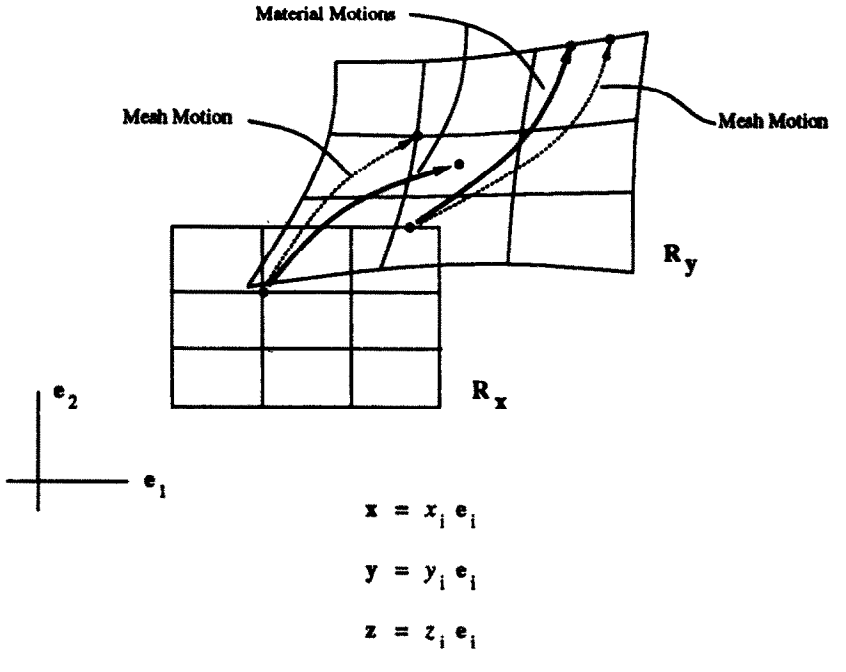

Fig. 1. Motions in arbitrary Lagrangian–Eulerian formulation.

Since their early applications in hydrodynamics codes [12], arbitrary Lagrangian–Eulerian formulations have been used in various problem areas. Let us summarize the key equations below.

Let $\mathscr{R}_x$ denote the initial configuration of the particles considered and $\mathscr{R}_y$ denote the current configuration. The coordinates of a material particle in these configurations are $\mathbf{x}$ and $\mathbf{y}$, respectively; hence we have $\mathbf{x} \in \mathscr{R}_x$ and $\mathbf{y} \in \mathscr{R}_y$ and

$$\mathbf{y} = \bar{\mathbf{y}}(\mathbf{x}, t). \tag{13}$$

Let $\mathbf{z}$ denote the coordinates of the points defined by the finite element mesh. Although not necessary, we assume that at time 0, the original body configuration $\mathscr{R}_x$ is identical with the original mesh configuration. Then we have with $\mathbf{z} \in \mathscr{R}_z$

$$\mathbf{y} = \hat{\mathbf{y}}(\mathbf{z}, t). \tag{14}$$

Figure 1 illustrates these concepts schematically, where we also assume that throughout the motion the boundary of the mesh is identical to the boundary of the body.

Consider a physical quantity f (e.g., density, particle velocity). To express this quantity in the Eulerian description we write

$$f = \bar{f}(\mathbf{y}, t) \tag{15}$$

while in the Lagrangian description we write

$$f = \bar{f}(\bar{\mathbf{y}}(\mathbf{x}, t), t) = \bar{f}(\mathbf{x}, t). \tag{16}$$

We then introduce the arbitrary Lagrangian–Eulerian description or the *mesh-referential description*, in which we associate the value of f with $\mathbf{z}$ via the mesh motion $\hat{\mathbf{y}}$, i.e.

$$f = \bar{f}(\hat{\mathbf{y}}(\mathbf{z}, t), t) = \hat{f}(\mathbf{z}, t). \tag{17}$$

In other words, we attach the variable f to mesh points.

In the Eulerian description, the time rate of change is the rate observed at a fixed point in space—*the spatial time derivative*—defined by

$$f' = \frac{\partial}{\partial t} \bar{f}(\mathbf{y}, t)|_{\mathbf{y}\ \text{fixed}} \tag{18}$$

whereas the time rate of change of f with respect to a fixed material particle—*the material time derivative*—is defined by

$$\dot{f} = \frac{\partial}{\partial t} \bar{f}(\mathbf{x}, t)|_{\mathbf{x}\ \text{fixed}} \tag{19}$$

and finally the time rate of change of f with respect to a given reference point $\mathbf{z} \in \mathscr{R}_z$ (or a given mesh point)—*the mesh-referential time derivative*—is defined by

$$f^* = \frac{\partial}{\partial t} \hat{f}(\mathbf{z}, t)|_{\mathbf{z}\ \text{fixed}}. \tag{20}$$

The spatial time derivative and the material time derivative are related by

$$\dot{f} = \frac{\partial \bar{f}(\mathbf{y}, t)}{\partial t} + \frac{\partial \bar{f}(\mathbf{y}, t)}{\partial y_i} \frac{\partial y_i}{\partial t}\bigg|_{\mathbf{y} = \bar{\mathbf{y}}(\mathbf{x}, t)}$$

$$= \frac{\partial \bar{f}(\mathbf{y}, t)}{\partial t} + \frac{\partial \bar{f}(\mathbf{y}, t)}{\partial \mathbf{y}} \cdot \frac{\partial \mathbf{y}}{\partial t}\bigg|_{\mathbf{y} = \bar{\mathbf{y}}(\mathbf{x}, t)} \tag{21}$$

or dropping $(\bar{\ })$ and $(\tilde{\ })$ and denoting the particle velocity $\partial \bar{\mathbf{y}}/\partial t$ by $\mathbf{v}$, we have

$$\dot{f} = f' + \operatorname{grad} f \cdot \mathbf{v}. \tag{22}$$

The convective term $\operatorname{grad} f \cdot \mathbf{v}$ arises from the fact that a fixed point in space $\mathbf{y}$ does not always represent the same material particle.

Using the mesh-referential time derivative and the spatial time derivative we obtain

$$f^* = \frac{\partial \bar{f}(\mathbf{y}, t)}{\partial t} + \frac{\partial \bar{f}(\mathbf{y}, t)}{\partial \mathbf{y}} \cdot \frac{\partial \mathbf{y}}{\partial t}\bigg|_{\mathbf{y} = \hat{\mathbf{y}}(\mathbf{z}, t)}$$

$$= f' + \operatorname{grad} f \cdot \mathbf{v}^m, \tag{23}$$

where $\mathbf{v}^m = \partial \hat{\mathbf{y}}/\partial t$ is the velocity of a mesh point. This equation is of key importance in the subsequent derivations.

From the above relation we see that if the mesh motion coincides with the material particle motion, i.e., $\mathbf{v}^m = \mathbf{v}$, the mesh-referential time derivative is identical to the material time derivative. On the other hand, if the mesh is fixed in space, i.e., $\mathbf{v}^m = \mathbf{0}$, then the mesh-referential time derivative and the spatial time derivative are identical.

In the ALE finite element formulation, the mesh motion $\hat{\mathbf{y}}$ is specified by some updating rule and is generally distinct from either zero or the particle motion. The time rate of change to be used is accordingly the mesh referential time derivative.

2.2. *ALE governing equations and weak forms*

We summarize below the Eulerian form of the equations governing an irrotational and isentropic flow of an inviscid fluid subject to conservative body forces

$$h + \phi' + \tfrac{1}{2}(\operatorname{grad} \phi)^2 - G = \lambda \quad \text{in } \mathscr{R}_y \tag{24}$$

$$\rho' + \operatorname{div}(\rho \operatorname{grad} \phi) = 0 \quad \text{in } \mathscr{R}_y \tag{25}$$

$$p = p(\rho) \quad \text{in } \mathscr{R}_y \tag{26}$$

$$\int_{\mathscr{R}_y} \rho \, dV_y = M \tag{27}$$

$$\frac{\partial \phi}{\partial n} = 0 \quad \text{on } \partial \mathscr{R}_y^E \tag{28}$$

$$\frac{\partial \phi}{\partial n} = \dot{u}_n \quad \text{on } \partial \mathscr{R}_y^M \tag{29}$$

$$\pi = -\bar{p} \quad \text{on } \partial \mathscr{R}_y^M, \tag{30}$$

where

ϕ = velocity potential
ρ = mass density
λ = unsteady Bernoulli's (spatial) constant, i.e., $\lambda = \lambda(t)$
u_n = normal boundary displacement
p = pressure
G = body force potential $= -gy_3$

$$h = \text{specific enthalpy} = \int \frac{dp}{\rho}$$

M = total mass of the fluid body
$\pi = \rho e + \rho\phi' + \frac{1}{2}\rho(\text{grad}\,\phi)^2 - \rho G - \rho\lambda$

$$e = \text{specific internal energy} = -\int p \, d\left(\frac{1}{\rho}\right)$$

$\bar{p}$ = prescribed pressure
$\partial \mathscr{R}_y^E$ = fixed part of the boundary of $\mathscr{R}_y$
$\partial \mathscr{R}_y^M$ = part of the boundary of $\mathscr{R}_y$ which is a moving material surface
$\mathbf{n}$ = positive inward surface normal vector corresponding to $\partial \mathscr{R}_y$.

The above set of equations can be obtained by taking the variation of [10]

$$\Pi(\rho, \phi, \lambda, u_n) = \int_t \left[\int_{\mathscr{R}_y} \pi \, dV_y + \lambda M \right] dt \tag{31}$$

given eqn (26) as a side constraint. Equation (24) is the unsteady Bernoulli equation, which is a scalar form of the momentum equations. Equation (25) is the continuity equation. Equation (26) is the state equation. Equation (27) is the global mass conservation equation, which is required in order to solve for λ. Equation (28) specifies zero flow across $\partial \mathscr{R}_y^E$. Nonzero flow can be included by letting $\rho \, \partial\phi/\partial n = \dot{m}$ on $\partial \mathscr{R}_y^E$ and

$$M = M_0 + \int_{\partial \mathscr{R}_y^E} \dot{m} \, dA_y,$$

where $\dot{m}$ is the prescribed mass flow rate and M_0 is the initial total mass. Equation (29) is the kinematic boundary condition at a free surface or a fluid–structure interface. The variable π can be shown, at equilibrium conditions, to be equal to the negative of the pressure, thus eqn (30) is the dynamic boundary condition which specifies the pressure on a moving material surface. We retain the form of eqn (30), instead of using $p(\rho) = \bar{p}$, since this form follows directly from the stationarity of Π.

The time derivatives that appear in the above equations are Eulerian time derivatives. To permit moving the finite element mesh, we transform these rates into mesh-referential time derivatives using eqn (23). Also, our assumption is that the boundaries of the fluid domain and the mesh coincide, so that the normal velocity of the mesh is equal to the normal velocity of the boundary or $\dot{u}_n = \dot{u}_n^m$. To underscore this fact we shall later write $\dot{u}_n^m$ instead of $\dot{u}_n$.

In the following formulation the state equation (26) is enforced by direct substitution, i.e., it is treated as a constitutive equation. With the above substitutions the weak forms of eqns (24) and (25) and (27)–(30) to be satisfied at any time t in the configuration $\mathscr{R}_y$ are

$$\int_{\mathscr{R}_y} \delta\rho [h + \phi^* - \mathbf{v}^m \cdot \text{grad}\,\phi + \tfrac{1}{2}(\text{grad}\,\phi)^2 + gy_3 - \lambda] \, dV_y = 0 \tag{32}$$

$$\int_{\mathscr{R}_y} [\delta\phi(-\rho^* + \mathbf{v}^m \cdot \text{grad}\,\rho) + \rho \, \text{grad}\,\phi \cdot \text{grad}\,\delta\phi] \times dV_y + \int_{\partial \mathscr{R}_y^M} \delta\phi \rho \dot{u}_n^m \, dA_y = 0 \tag{33}$$

$$\delta\lambda \int_{\mathscr{R}_y} \rho \, dV_y = \delta\lambda M \tag{34}$$

$$\int_{\partial \mathscr{R}_y^M} \delta u_n^m \pi \, dA_y = -\int_{\partial \mathscr{R}_y^M} \delta u_n^m \bar{p} \, dA_y. \tag{35}$$

An updating rule for the interior values of $\mathbf{u}^m$ and the tangential component of the boundary motion are required, either in a form of constraint equations or an updating algorithm relating $\mathbf{u}^m$ to u_n^m.

2.3. *Linearization and finite element discretization*

The weak forms derived in the preceding section can be written symbolically as

$$\delta W(\theta) = \delta R, \tag{36}$$

where $\theta = (\rho, \phi, \lambda, \mathbf{u}^m, \rho^*, \phi^*, \mathbf{v}^m)$, δW is the sum of the left-hand sides of the weak forms—the 'internal virtual work', and δR is the sum of the right-hand sides of the weak forms—the 'external virtual work'.

Applying finite element interpolations on θ yields the discretized equilibrium equations

$$\mathbf{F}(\boldsymbol{\Theta}) = \mathbf{R}, \tag{37}$$

where $\boldsymbol{\Theta}$ is a vector containing nodal values of θ and $\mathbf{F}$ depends nonlinearly on $\boldsymbol{\Theta}$.

Assume that the solution up to time t is known and we want to find the solution for time $t + \Delta t$. We can write the Taylor series expansion of eqn (37) in the configuration at time t as

$$^{t+\Delta t}\mathbf{R} = \mathbf{F}(^{t+\Delta t}\boldsymbol{\Theta}) \doteq \mathbf{F}(^{t}\boldsymbol{\Theta}) + \left.\frac{\partial \mathbf{F}}{\partial \boldsymbol{\Theta}}\right|_{t\Theta} \cdot \Delta\boldsymbol{\Theta} \tag{38}$$

and the tangent stiffness and coupling matrices can be determined from $\partial\mathbf{F}/\partial\boldsymbol{\Theta}$.

Since

$$\frac{\partial \mathbf{F}}{\partial \boldsymbol{\Theta}} \cdot \Delta\boldsymbol{\Theta} = \frac{\partial \mathbf{F}}{\partial \boldsymbol{\Theta}} \cdot \frac{\partial \boldsymbol{\Theta}}{\partial t}\,\Delta t \tag{39}$$

and the variables in $\boldsymbol{\Theta}$ are attached to mesh points (nodal points) it follows that

$$\frac{\partial \mathbf{F}}{\partial \boldsymbol{\Theta}} \cdot \Delta\boldsymbol{\Theta} = \mathbf{F}^{*}\Delta t. \tag{40}$$

Thus

$$\mathbf{F}(^{t}\boldsymbol{\Theta}) + \mathbf{F}^{*}|_{t}\Delta t \doteq {}^{t+\Delta t}\mathbf{R} \tag{41}$$

and similarly

$$\delta^{t}W + \delta W^{*}|_{t}\Delta t \doteq \delta^{t+\Delta t}R. \tag{42}$$

Thus far the linearization was performed on an equilibrium configuration at time t but the results above are equally applicable to a 'non-equilibrium configuration' as encountered in the Newton iteration method in which the tangent matrix is recalculated in every iteration.

Considering the parts of δW corresponding to $\delta\rho$, we obtain from eqn (32)

$$\begin{aligned}\delta W^{*}_{\rho}\Delta t = \int_{\mathscr{R}_y} \{&\delta\rho\{\Delta h + \Delta\phi^{*} - \Delta\mathbf{v}^{m}\cdot\operatorname{grad}\phi\\ &+ (\operatorname{grad}\phi - \mathbf{v}^{m})\cdot[-\operatorname{grad}^{T}(\Delta\mathbf{u}^{m})\operatorname{grad}\phi\\ &+ \operatorname{grad}(\Delta\phi)] + g\Delta y_3 - \Delta\lambda\}\\ &+ \delta\rho\,\operatorname{div}(\Delta\mathbf{u}^{m})\sigma\}\,\mathrm{d}V_y,\end{aligned} \tag{43}$$

where

$$\sigma = h + \phi^{*} - \mathbf{v}^{m}\cdot\operatorname{grad}\phi + \tfrac{1}{2}(\operatorname{grad}\phi)^2 + gy_3 - \lambda. \tag{44}$$

From eqn (33) we obtain

$$\begin{aligned}\delta W^{*}_{\phi}\Delta t = \int_{\mathscr{R}_y} \{&\delta\phi\{-\Delta\rho^{*} + \Delta\mathbf{v}^{m}\cdot\operatorname{grad}\rho\\ &+ \mathbf{v}^{m}\cdot[-\operatorname{grad}^{T}(\Delta\mathbf{u}^{m})\operatorname{grad}\rho\\ &+ \operatorname{grad}(\Delta\rho)]\} + \rho\operatorname{grad}\delta\phi\\ &\cdot[-\operatorname{grad}^{T}(\Delta\mathbf{u}^{m})\operatorname{grad}\phi + \operatorname{grad}(\Delta\phi)]\\ &+ \Delta\rho\operatorname{grad}\phi\cdot\operatorname{grad}\delta\phi + \rho\operatorname{grad}\phi\\ &\cdot[-\operatorname{grad}^{T}(\Delta\mathbf{u}^{m})\operatorname{grad}\delta\phi]\\ &+ \operatorname{div}(\Delta\mathbf{u}^{m})[\delta\phi(-\rho^{*} + \mathbf{v}^{m}\cdot\operatorname{grad}\rho)\\ &+ \rho\operatorname{grad}\phi\cdot\operatorname{grad}\delta\phi]\}\,\mathrm{d}V_y\\ &+ \int_{\partial\mathscr{R}^{M}_{y}} [\delta\phi(\Delta\rho\mathbf{v}^{m} + \rho\Delta\mathbf{v}^{m})\\ &+ \delta\phi\operatorname{div}(\Delta\mathbf{u}^{m})\rho\mathbf{v}^{m}\\ &- \delta\phi\rho\operatorname{grad}(\Delta\mathbf{u}^{m})\mathbf{v}^{m}]\cdot\mathbf{n}\,\mathrm{d}A_y.\end{aligned} \tag{45}$$

From eqn (34) we obtain

$$\delta W^{*}_{\lambda}\Delta t = \delta\lambda\int_{\mathscr{R}_y} [\Delta\rho + \rho\operatorname{div}(\Delta\mathbf{u}^{m})]\,\mathrm{d}V_y. \tag{46}$$

Finally from eqn (35) we have

$$\begin{aligned}\delta W^{*}_{u^{m}}\Delta t = \int_{\partial\mathscr{R}^{M}_{y}} \{&\delta\mathbf{u}^{m}\sigma\Delta\rho + \delta\mathbf{u}^{m}\rho\{\Delta\phi^{*} - \Delta\mathbf{v}^{m}\\ &\cdot\operatorname{grad}\phi + (\operatorname{grad}\phi - \mathbf{v}^{m})\\ &\cdot[-\operatorname{grad}^{T}(\Delta\mathbf{u}^{m})\operatorname{grad}\phi + \operatorname{grad}(\Delta\phi)]\\ &+ g\Delta y_3 - \Delta\lambda\} + \pi[\operatorname{div}(\Delta\mathbf{u}^{m})\mathbf{1}\\ &- \operatorname{grad}(\Delta\mathbf{u}^{m})]\,\delta\mathbf{u}^{m}\}\cdot\mathbf{n}\,\mathrm{d}A_y.\end{aligned} \tag{47}$$

Although it is possible to simplify the above expressions using the equilibrium conditions at time t, we retain the above forms so that the corresponding tangent matrices be applicable as well in a non-equilibrium configuration.

Applying a standard discretization procedure [11] with

$$\rho = \mathbf{H}_{\rho}\boldsymbol{\rho} \tag{48}$$

$$\phi = \mathbf{H}_{\phi}\boldsymbol{\Phi} \tag{49}$$

$$\mathbf{u} = \mathbf{H}\mathbf{U}, \tag{50}$$

where ρ, Φ, and U contain the nodal values of ρ, ϕ, and $\mathbf{u}^m$, respectively, we directly obtain the following matrix equations

$$^t\mathbf{K}\Delta\Psi + {}^t\mathbf{C}\Delta\dot{\Psi} = {}^{t+\Delta t}\mathbf{R} - {}^t\mathbf{F}, \tag{51}$$

where

$$\Psi \begin{bmatrix} \rho \\ \Phi \\ \lambda \\ \mathbf{U}^B \\ \mathbf{U}^I \end{bmatrix} \tag{52}$$

$$^t\mathbf{K} = \begin{bmatrix} \mathbf{K}_{\rho\rho} & \mathbf{K}_{\rho\phi} & \mathbf{K}_{\rho\lambda} & \mathbf{K}_{\rho u^B} & \mathbf{K}_{\rho u^I} \\ \mathbf{K}_{\phi\rho} & \mathbf{K}_{\phi\phi} & \mathbf{0} & \mathbf{K}_{\phi u^B} & \mathbf{K}_{\phi u^I} \\ \mathbf{K}_{\lambda\rho} & \mathbf{0} & \mathbf{0} & \mathbf{K}_{\lambda u^B} & \mathbf{K}_{\lambda u^I} \\ \mathbf{K}_{u^B\rho} & \mathbf{K}_{u^B\phi} & \mathbf{K}_{u^B\lambda} & \mathbf{K}_{u^Bu^B} & \mathbf{K}_{u^Bu^I} \\ \mathbf{0} & \mathbf{0} & \mathbf{0} & \mathbf{0} & \mathbf{0} \end{bmatrix} \tag{53}$$

$$^t\mathbf{C} = \begin{bmatrix} \mathbf{0} & \mathbf{C}_{\rho\phi} & \mathbf{0} & \mathbf{C}_{\rho u^B} & \mathbf{C}_{\rho u^I} \\ \mathbf{C}_{\phi\rho} & \mathbf{0} & \mathbf{0} & \mathbf{C}_{\phi u^B} & \mathbf{C}_{\phi u^I} \\ \mathbf{0} & \mathbf{0} & \mathbf{0} & \mathbf{0} & \mathbf{0} \\ \mathbf{0} & \mathbf{C}_{u^B\phi} & \mathbf{0} & \mathbf{C}_{u^Bu^B} & \mathbf{0} \\ \mathbf{0} & \mathbf{0} & \mathbf{0} & \mathbf{0} & \mathbf{0} \end{bmatrix}. \tag{54}$$

In the above equations $\mathbf{K}_{\rho\rho}$ and $\mathbf{K}_{\phi\phi}$ are symmetric, $\mathbf{K}_{\lambda\rho} = \mathbf{K}_{\rho\lambda}^T$, $\mathbf{C}_{\phi\rho} = -\mathbf{C}_{\rho\phi}^T$, and subscripts u^B and u^I refer to the $\mathbf{u}^m$ degrees of freedom corresponding to boundary points and interior points, respectively. The matrices are obtained from eqns (43)–(47) in the standard manner.

We note that if 'linear conditions' are assumed, the stiffness and coupling matrices can be reduced to those previously given in eqn (11).

Now that the linearized equilibrium equations are established in eqn (51) we can choose a suitable time integration scheme to analyze a given problem.

2.4. *Boundary conditions and mesh updating*

To solve for the response of the fluid using the above equations, the mesh motion $\hat{\mathbf{y}}$ must be defined. Considering the definition of the mesh motion, two conditions must be met on the fluid–structure interface; the force equilibrium condition

$$p^f\mathbf{n}^f = \boldsymbol{\tau}^s\mathbf{n}^s \tag{55}$$

and the compatibility condition, in case no separation is allowed

$$\mathbf{u}^f \cdot \mathbf{n}^f = -\mathbf{u}^s \cdot \mathbf{n}^s, \tag{56}$$

where the superscripts f and s denote the fluid and solid, respectively. On a totally submerged interface with no separation the two conditions can be met by simply attaching the ALE fluid nodes to the Lagrangian structural nodes. Using the same nodes and shape functions along the boundary ensures the compatibility condition while the finite element equations enforce the force equilibrium condition. The advantage of using the ALE formulation is evident in this case.

If the interface is partially submerged, the fluid node common to the free surface and the fluid–structure interface cannot be attached to the Lagrangian structural node without violating the kinematic and dynamic boundary conditions on the free surface. In addition, other nodes along the interface should be allowed to move from the solid nodes to preserve mesh regularity. Therefore, when the solid is modelled by a Lagrangian formulation a contact algorithm must be introduced to enforce the above two conditions.

On a free surface the boundary conditions involve only the fluid, and both the dynamic and the kinematic boundary conditions are embedded in the given formulation. However, the dynamic boundary condition only provides an equation for the motion normal to the free surface. An additional rule must be used to define the mesh motion in the tangential direction, and for many problems a natural choice is to set this motion equal to zero.

For interior nodes, the mesh motion should be chosen so as to prevent excessive mesh distortion. For a wide range of applications, this can be achieved by simply constraining the interior nodes to move in proportion to the boundary nodes, and we have used this approach in the problem solutions given next.

3. NUMERICAL EXAMPLES

The proposed formulation has been implemented experimentally in ADINA. The following five cases are chosen to demonstrate the capability of the formulation. Full Newton iterations have been employed in all cases, and the trapezoidal rule has been used for the transient time integrations.

3.1. *Steady compressible flow through a varying section channel*

We consider the subsonic steady isentropic flow of a perfect gas through a channel of variable cross-section. As shown in Fig. 2, the channel under consideration is 1 m wide at the inlet and 0.5 m wide at the outlet. The initial density, initial sound wave speed, and the perfect gas constant are 1.21 kg/m^3, 343 m/sec and 1.4, respectively. Figure 3 shows the mesh of 10 nine-node elements used in this case. All nodes are fixed in space and thus the formulation reduces to a

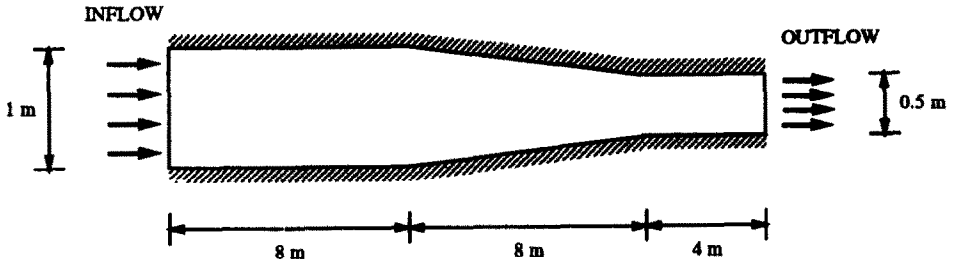

Fig. 2. Steady compressible flow through a varying cross-section channel problem.

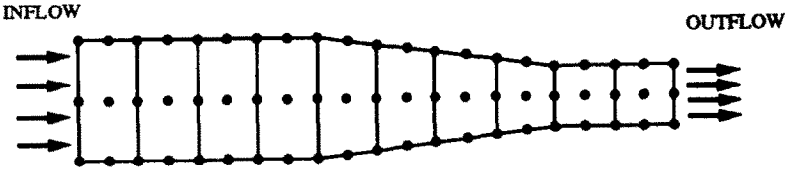

Fig. 3. Flow through a varying cross-section channel; mesh configuration.

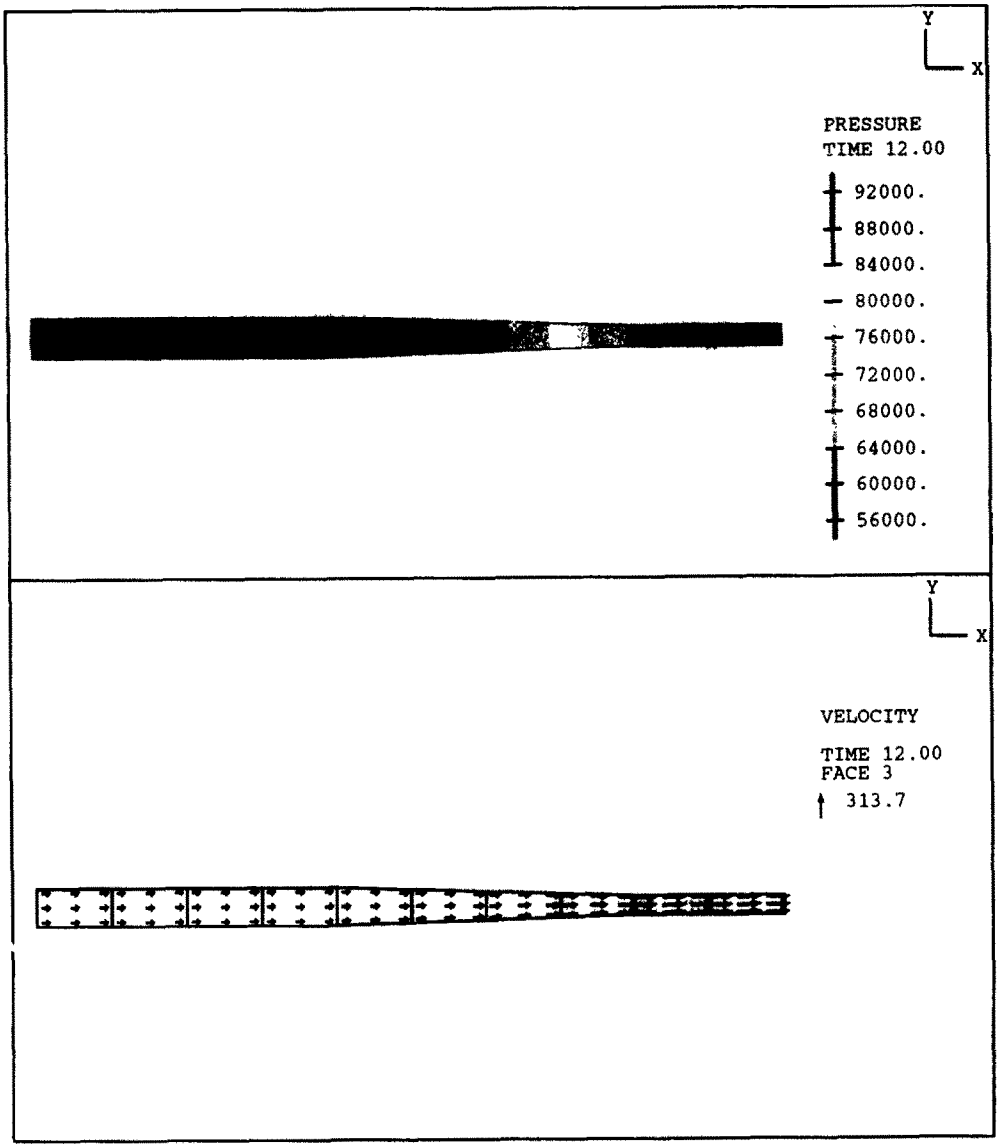

Fig. 4. Flow through a varying cross-section channel; pressure and velocity distribution corresponding to a mass flow rate of 120 kg/sec.

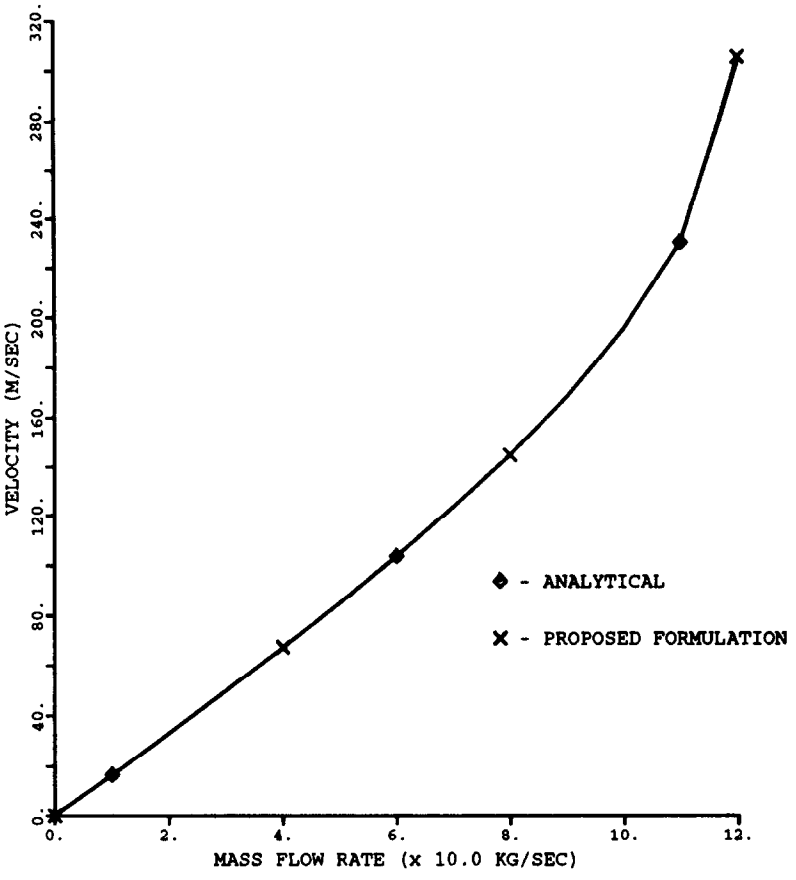

Fig. 5. Flow through a varying cross-section channel; relation between the flow rate and the downstream velocity.

purely Eulerian formulation. Since the gas is compressible we assign both velocity potential and density degrees of freedom to each node. The mass flow rate at the inlet is prescribed by applying a suitable 'force' on the inlet surface. The force vector, R_ϕ, corresponding to a mass flow rate of $\dot{m}$ is given by

$$R_\phi = \int_{\partial\Omega_y^E} \delta\phi \dot{m}\, \mathrm{d}A_y. \tag{57}$$

A uniform pressure condition is prescribed at the outlet by fixing the velocity potential degrees of freedom along the outlet surface.

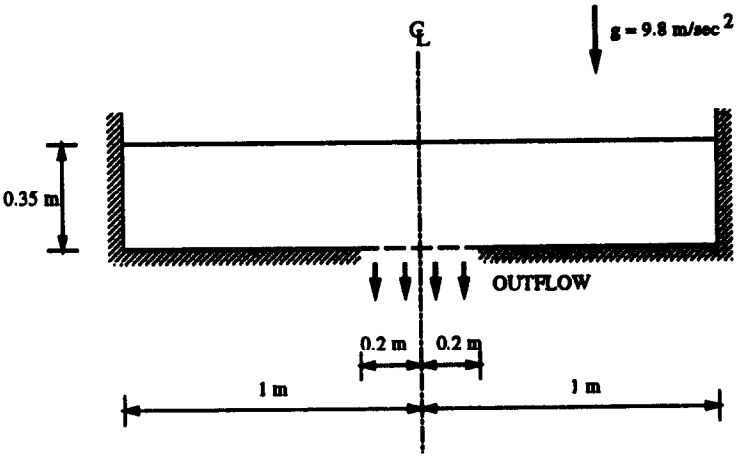

Fig. 6. Circular tank draining problem.

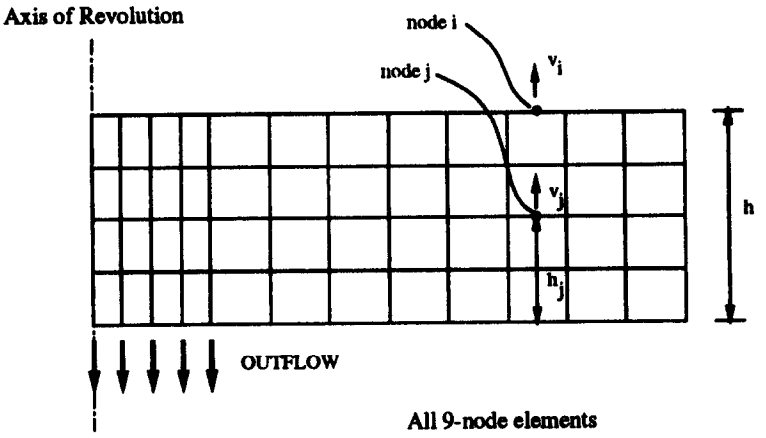

Fig. 7. Circular tank draining; initial mesh configuration.

The problem was analyzed by Kock and Olson [10] and the results agree well with the analytical solution (see, for example, [13]). Since our formulation reduces to that introduced by Kock and Olson for a Eulerian mesh, we expect similar results from our formulation. Figure 4 shows the pressure and the velocity distributions corresponding to a mass flow rate of 120 kg/sec. The relation between the mass flow rate and the downstream velocity is given in Fig. 5. The numerical solution is within 0.01% of the analytical solution.

3.2. *Circular tank draining of an incompressible fluid*

We now consider the draining of an incompressible fluid from an open cylindrical tank through a circular opening at the bottom of the tank. The tank radius is 1 m, the depth of the fluid is 0.35 m and the

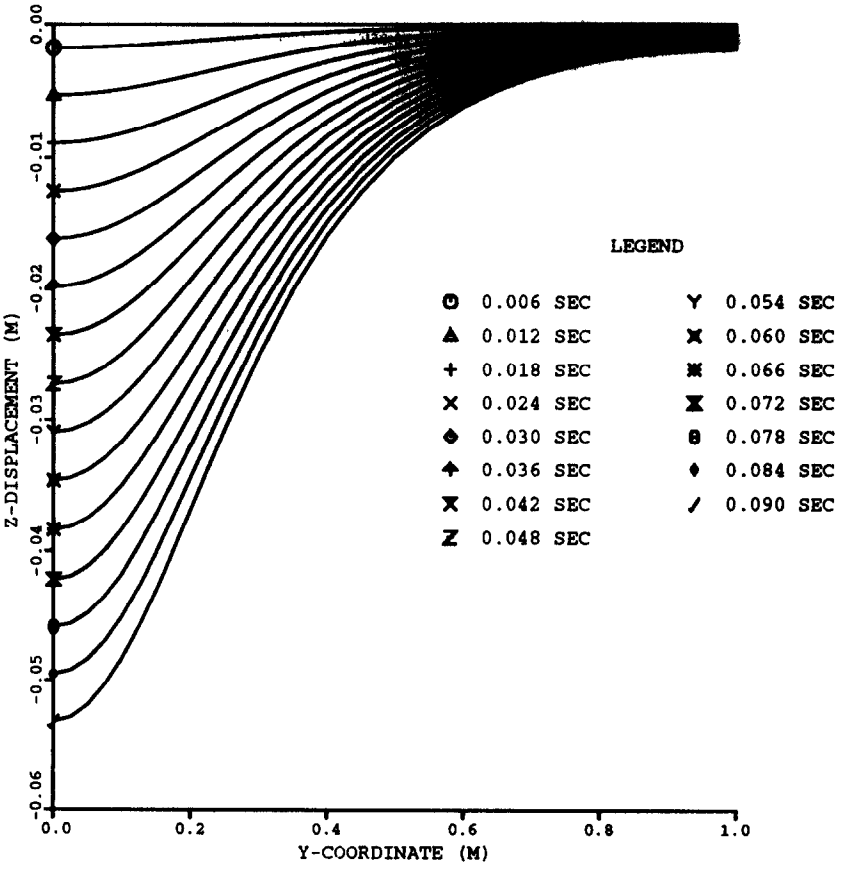

Fig. 8. Circular tank draining; free surface shapes at various times.

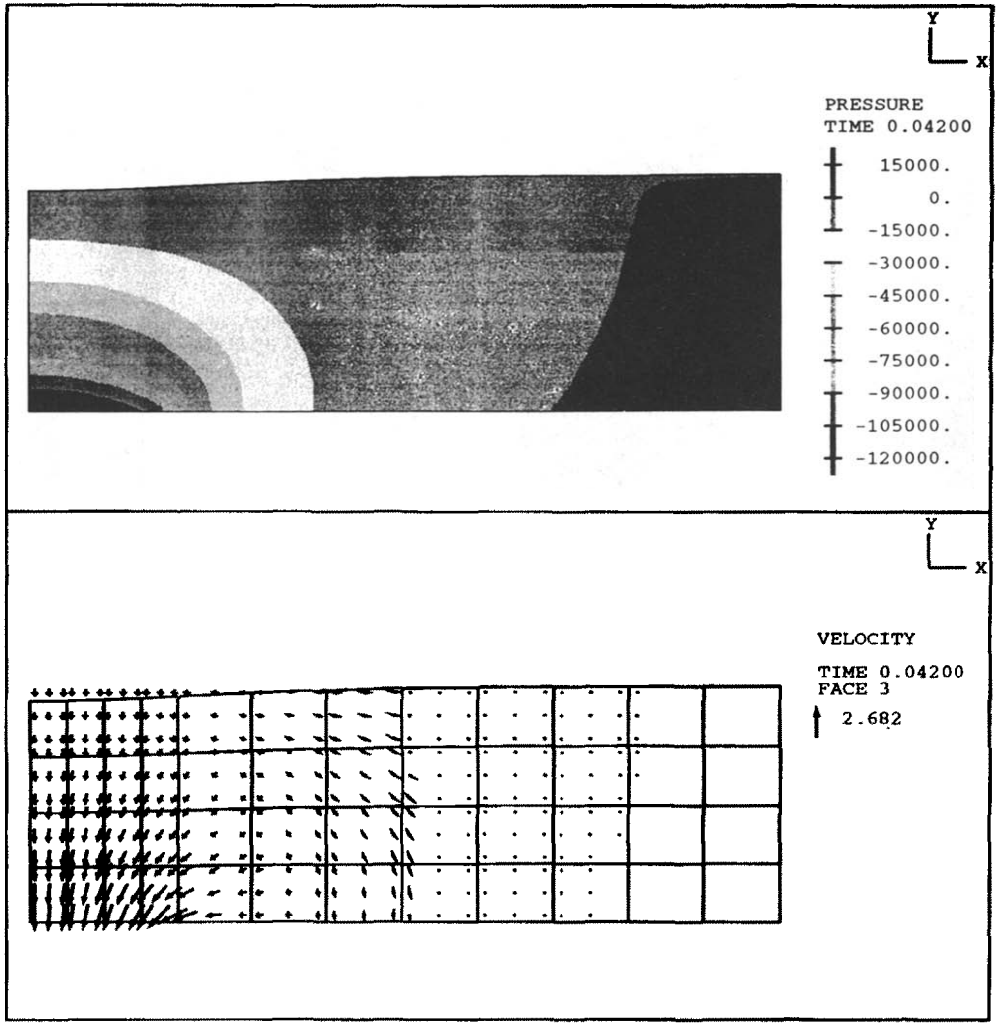

Fig. 9. Circular tank draining; pressure and velocity distributions at $t = 0.042$ sec.

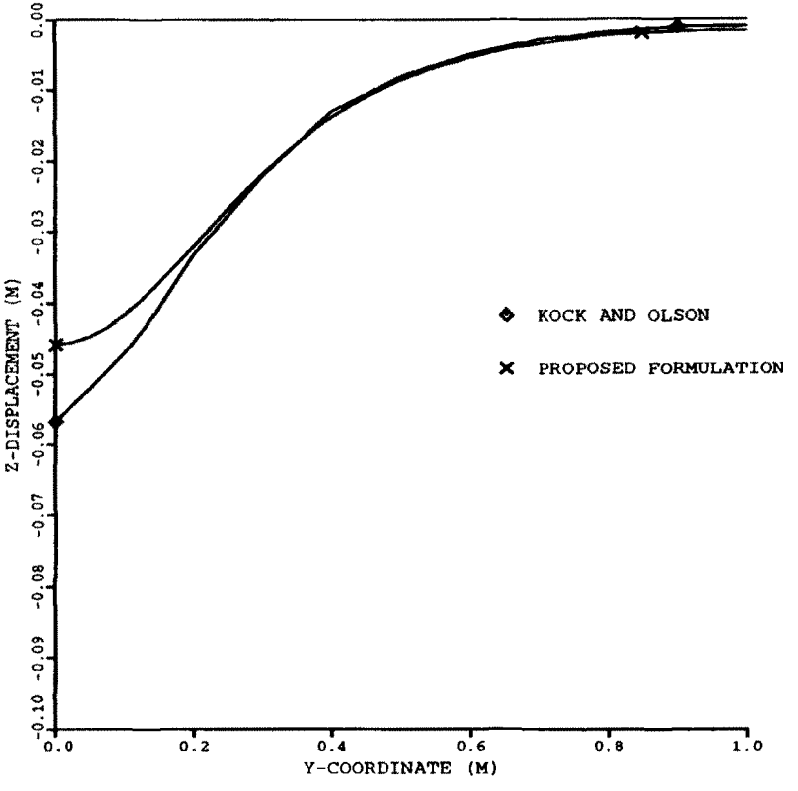

Fig. 10. Circular tank draining, free surface position at $t = 0.078$ sec.

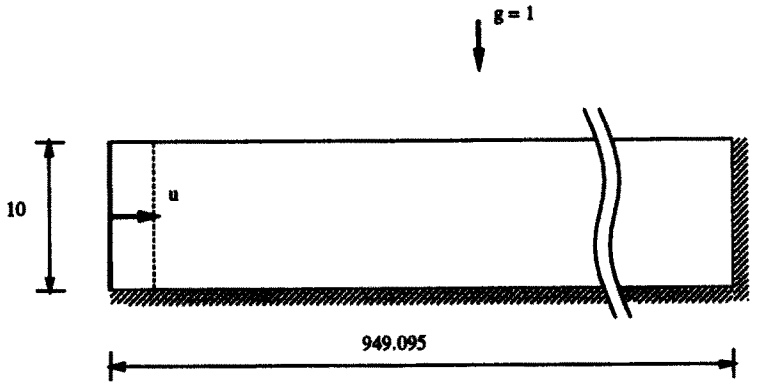

Fig. 11. Free surface wave propagation problem.

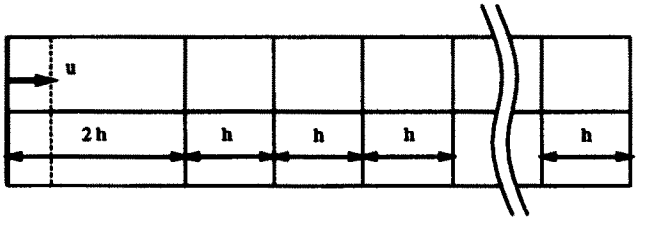

h=5.895

All 4-node elements, 64 elements along length

Fig. 12. Free surface wave propagation; initial mesh configuration.

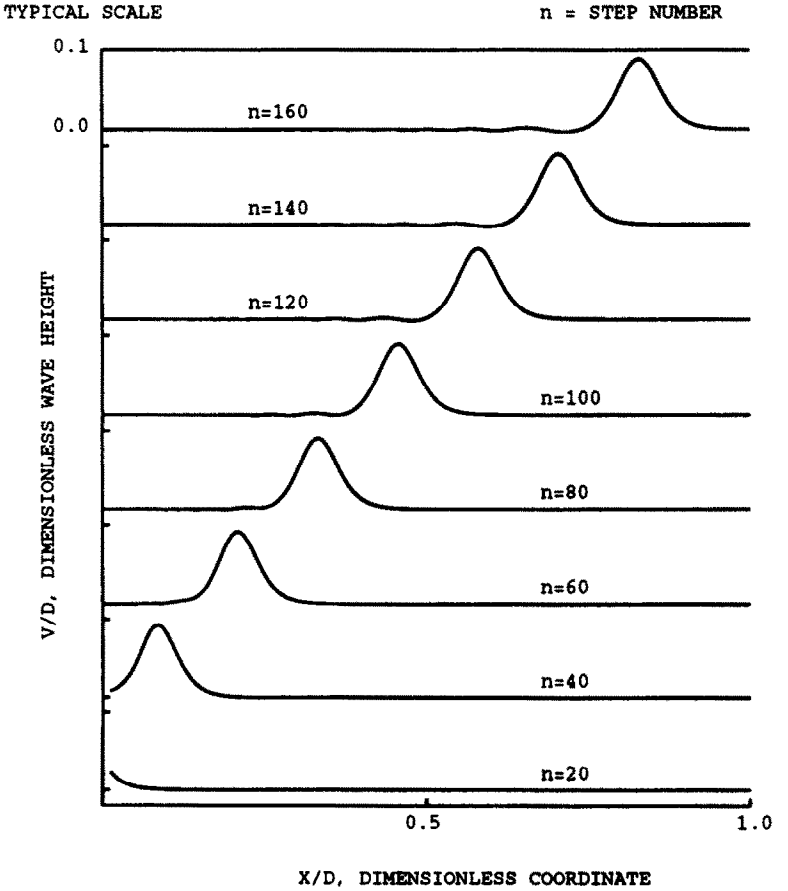

Fig. 13. Free surface wave propagation; free surface profiles at various times.

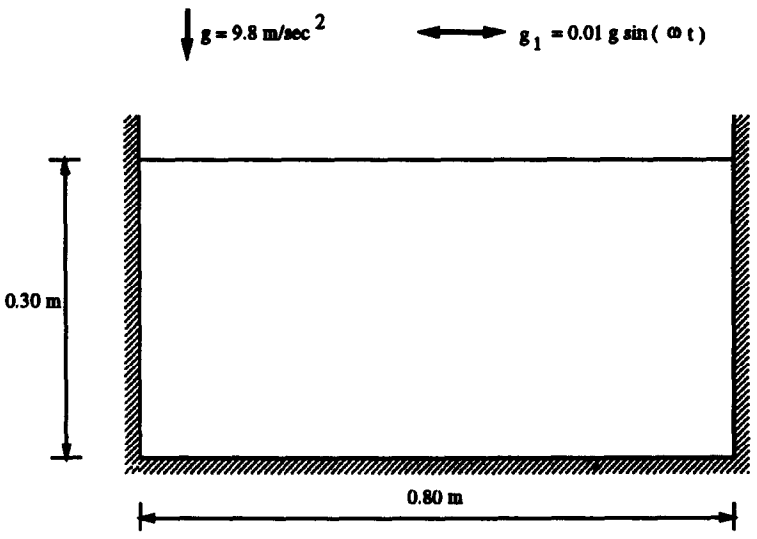

Fig. 14. Large amplitude sloshing problem.

specified flowrate out of the 0.2 m radius opening is 0.31 m^3/sec (see Fig. 6).

The finite element model used to analyze this problem is shown in Fig. 7. In this problem no density degree of freedom is required because the density of an incompressible fluid is constant. The whole mesh region is modelled as an ALE mesh and all nodes are horizontally fixed. Therefore, vertical displacement degrees of freedom are assigned to the nodes in addition to the velocity potential degrees of freedom. The nodes not on the free surface are constrained to move vertically in proportion to the vertical displacement of the free surface and the distance from the bottom of the tank, i.e., for a typical node j and the corresponding node i on the free surface

$$v_j = \frac{h_j}{h} v_i. \tag{58}$$

For the time integration, the trapezoidal rule was used with a time step of 0.006 sec.

The calculated shapes of the free surface at different times are plotted in Fig. 8. Figure 9 shows the pressure and the velocity distributions at time 0.042 sec.

The result at 0.078 sec is compared in Fig. 10 with the solution presented by Kock and Olson [10]. We observe that the formulation used in this reference predicts a dip near the center of the tank deeper than our formulation predicts. The discrepancies can be explained by the observation that Kock and Olson used a purely Eulerian formulation neglecting the convective terms due to the motion of the particles on the free surface.

3.3. *Free surface wave propagation*

In this problem chosen from [14] we consider a bed of an incompressible fluid as shown in Fig. 11 under

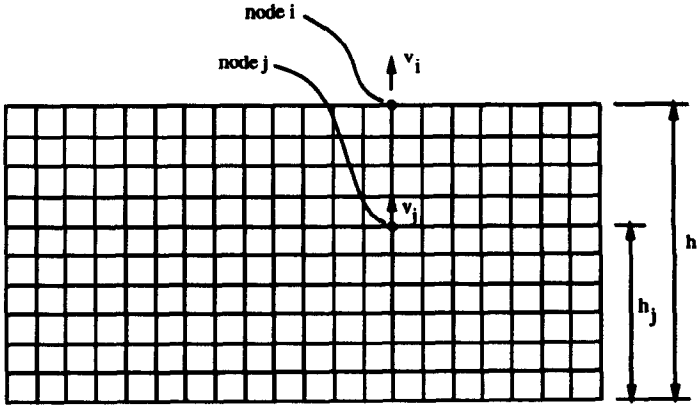

Fig. 15. Large amplitude sloshing; initial mesh configuration.

the passing of a solitary wave. The wave is generated by subjecting the left-hand boundary of the fluid to a horizontal displacement of

$$u = \frac{H}{\kappa}\left[1 + \tanh\left(\frac{c\kappa t}{D} - 4\right)\right], \tag{59}$$

where

$$c = \sqrt{gD\left(1 + \frac{H}{D}\right)}$$

$$\kappa = \sqrt{\frac{3H}{4D}}.$$

For this specific case we take $g = 1$, $L = 949.095$, $D = 10$, $H = 0.86$, and $\rho = 1$. The finite element mesh used in the analysis is shown in Fig. 12. The typical element width, h, was 5.895 and the time step employed was $\Delta t = h/c = 1.7888$.

Figure 13 shows the profile of the free surface at different times. The results agree well with those provided by Hughes *et al.* [14].

3.4. *Large amplitude sloshing*

The sloshing behavior of fluids is of key importance in studying the response of liquid-filled containers and nuclear reactor systems under seismic loading. This example chosen from [15] demonstrates the capability of the proposed formulation to analyze large amplitude sloshing.

The 0.8 m wide rigid container shown in Fig. 14 is filled with water to a depth of 0.3 m and then

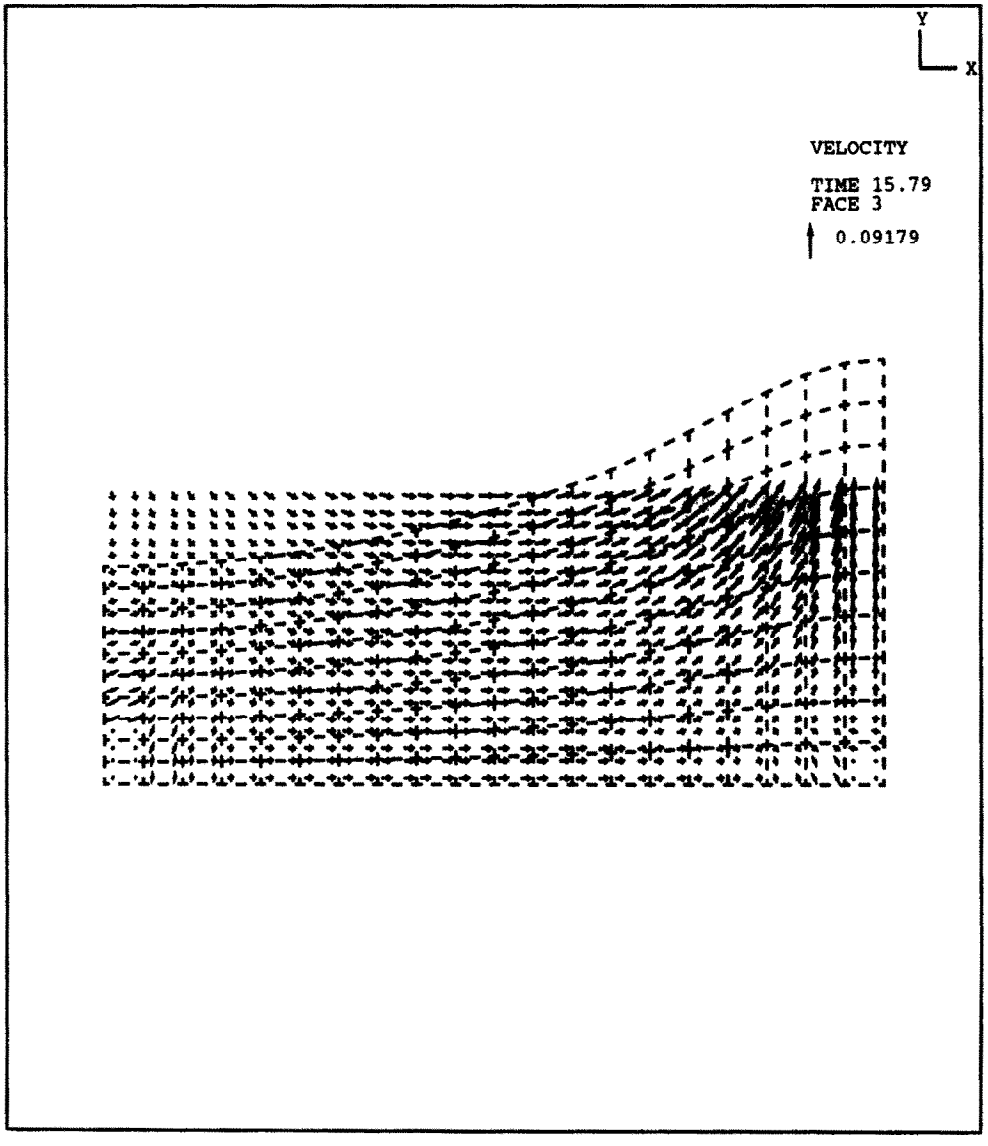

Fig. 16. Large amplitude sloshing; velocity distribution at $t = 15.7866$ sec.

excited for 10 cycles by a horizontal ground acceleration of

$$g_1 = Ag \sin(\omega t), \tag{60}$$

where $A = 0.01$, $g = 9.8$ m/sec^2, and $\omega/2\pi = 0.89$ Hz. The chosen frequency is approximately the fundamental frequency of the system. The mesh of four-node elements is shown in Fig. 15. The time step used was $\Delta t = 0.05618$ sec.

The velocity distributions at time 15.7866 sec and time 16.0675 sec are shown in Figs 16 and 17, respectively. The changing profiles of the free surface during the last 10 time steps are plotted in Fig. 18 and the time history of the vertical displacement experienced by the nodes at both ends of the free surface is given in Fig. 19. Due to nonlinearity, the amplitudes of the upward displacement at both ends of the free surface are of almost twice the magnitude of those of the corresponding downward displacement. If a linear theory were employed, the same magnitude would have been predicted for both the upward and the downward motion. These observations agree well with those obtained experimentally by Muto *et al.* [16] and numerically by Huerta and Liu [15].

3.5. *Gas bubble expanding in a water tank*

To demonstrate the capability of the formulation to analyze complex fluid–structure interactions, we consider the problem of a gas bubble bursting in a water tank, as shown in Fig. 20. The tank bottom and the upper part of the tank wall are rigid. The lower part of the tank wall (0.240 m high) is made of

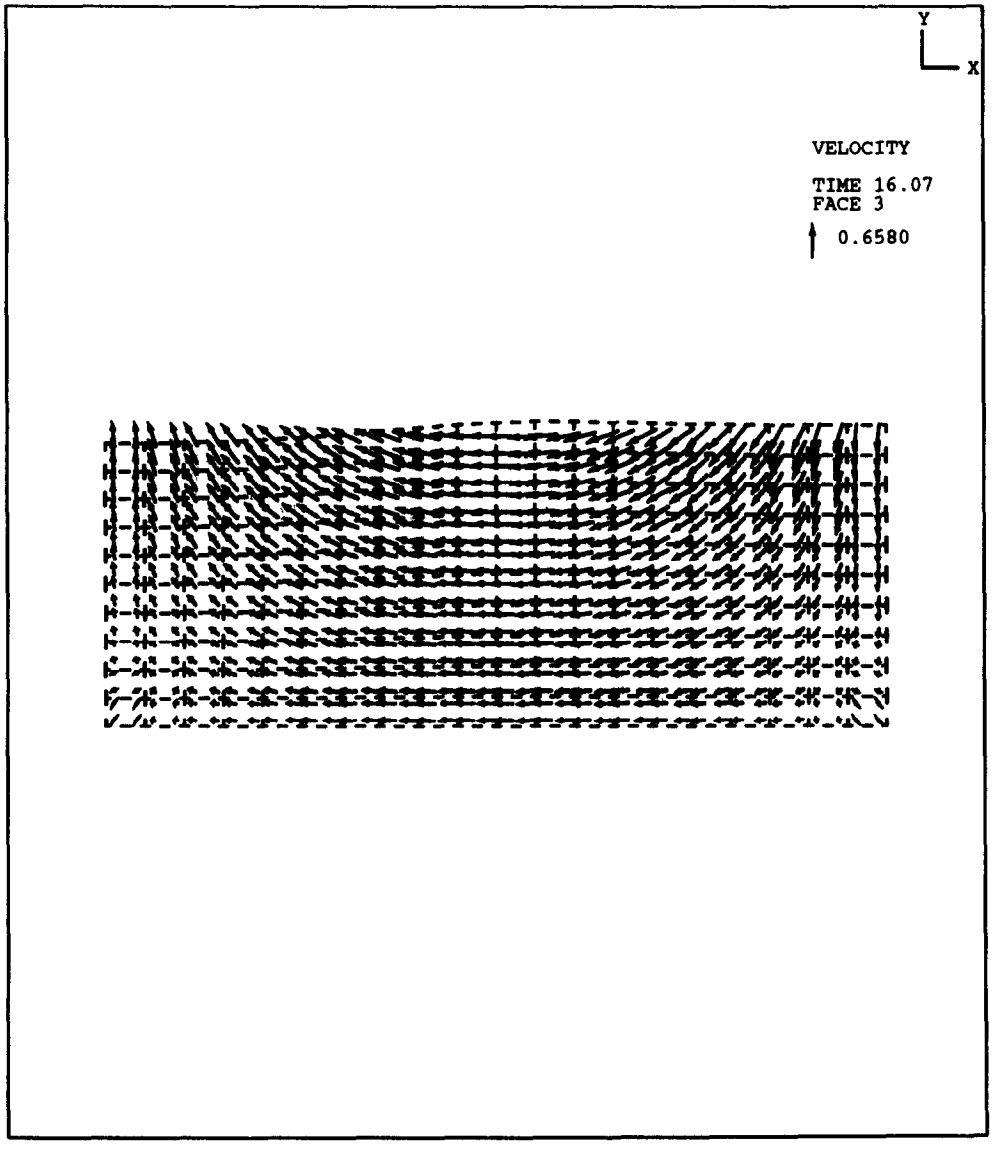

Fig. 17. Large amplitude sloshing; velocity distribution at $t = 16.0675$ sec.

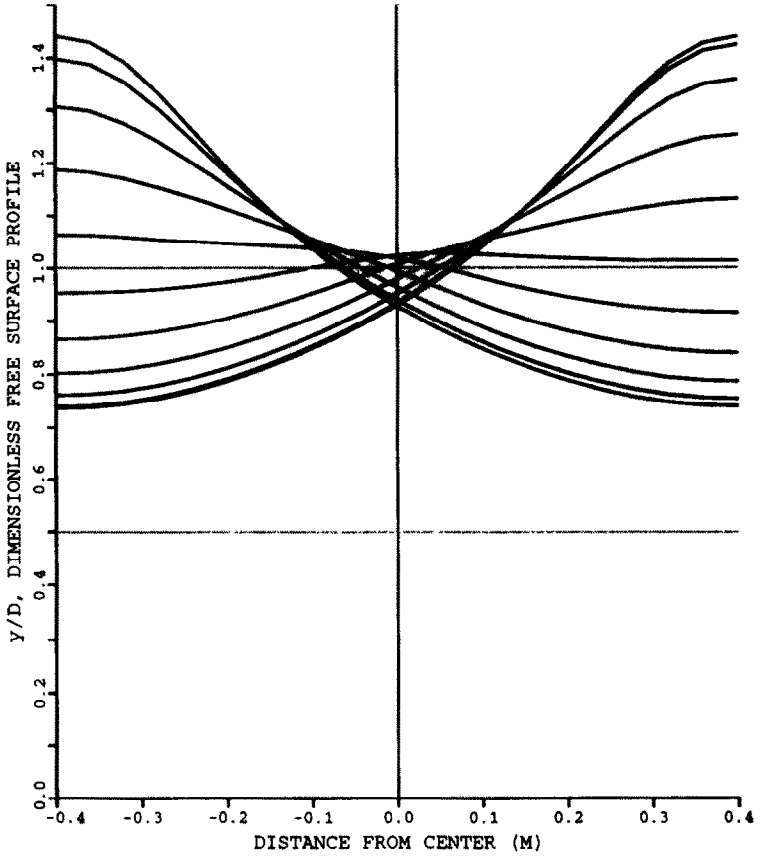

Fig. 18. Large amplitude sloshing; free surface profiles during the last 10 time steps.

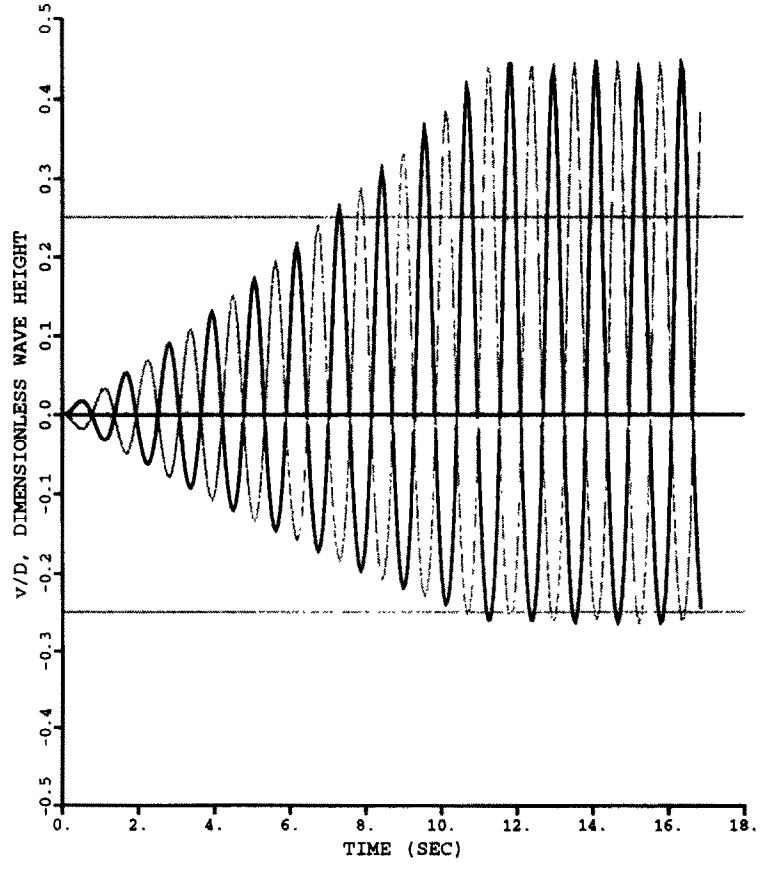

Fig. 19. Large amplitude sloshing; time history of the free surface displacements at the tank walls.

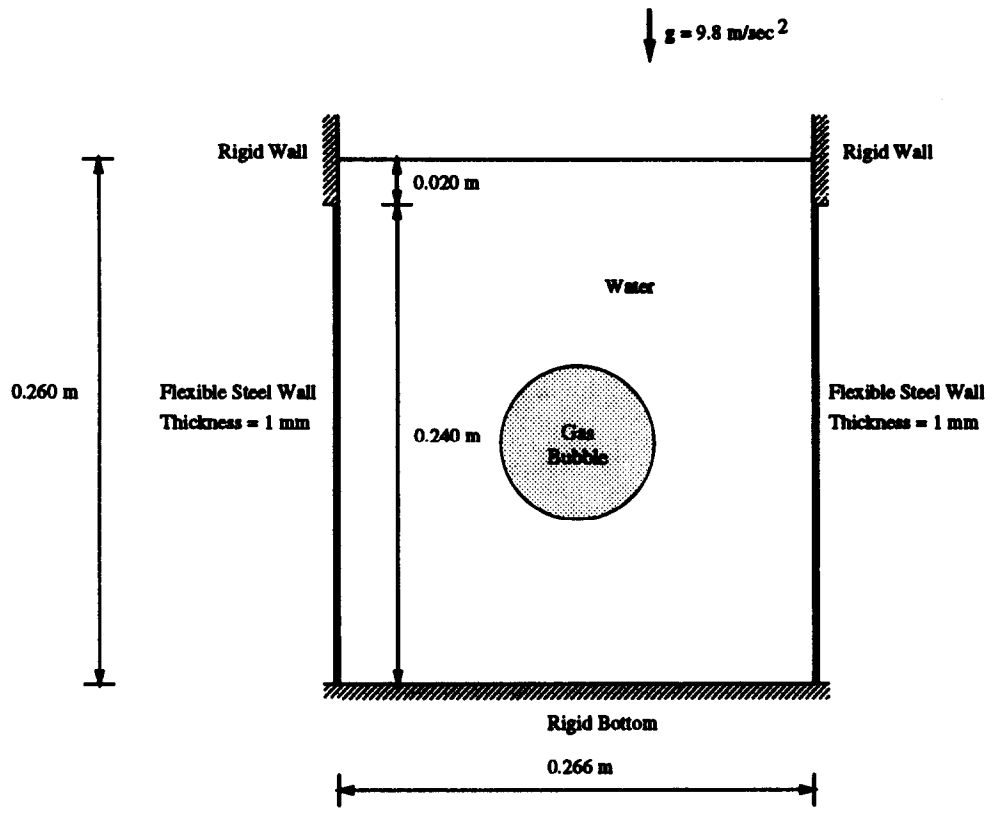

Fig. 20. The problem of a gas bubble expanding in a water tank.

a 1 mm thick steel plate. The gas contained in the bubble has an initial density of 270 kg/m^3 and an initial pressure of 162.9 MPa. In this problem solution we have no comparison results and therefore only want to demonstrate some modeling possibilities.

The initial configuration of the coarse mesh used in the analysis is shown in Fig. 21. Nodes along the water–gas interface are constrained to move in directions radial to the center of the gas bubble in the initial configuration. Interior nodes are constrained to move in proportion to the boundary nodes.

The time step used for the time integration was $\Delta t = 1 \times 10^{-5}$ sec. The mesh configurations and the water velocity distributions at the times 1×10^{-4}, 2×10^{-4}, and 3×10^{-4} sec are shown in Figs 22–24, respectively. Despite the relatively coarse mesh employed, the formulation works well in this complex situation involving large boundary motions.

4. CONCLUDING REMARKS

We presented a nonlinear U–ϕ–ρ–λ arbitrary Lagrangian–Eulerian formulation in which both the velocity potential, ϕ, and the density, ρ, are employed as variables at each fluid node. The linear form of the U–ϕ–ρ–λ formulation is equivalent to the velocity potential formulation and thus the method can be thought of as an extension of the work of Olson and Bathe [9]. The arbitrary Lagrangian–Eulerian approach adopted provides the formulation and the capability to solve problems in which the fluid undergoes very large boundary motions. The method has been shown to work equally well for both compressible and incompressible fluids. A particularly interesting issue left for further research is the modeling of partially submerged fluid–structure interfaces.

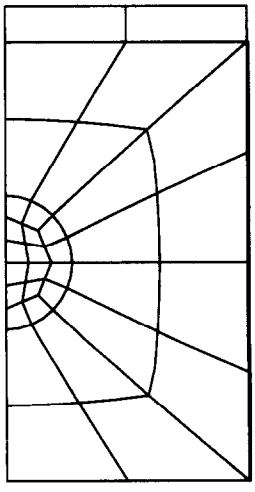

Fig. 21. Gas bubble expanding in a water tank; initial mesh configuration, nine-node elements.

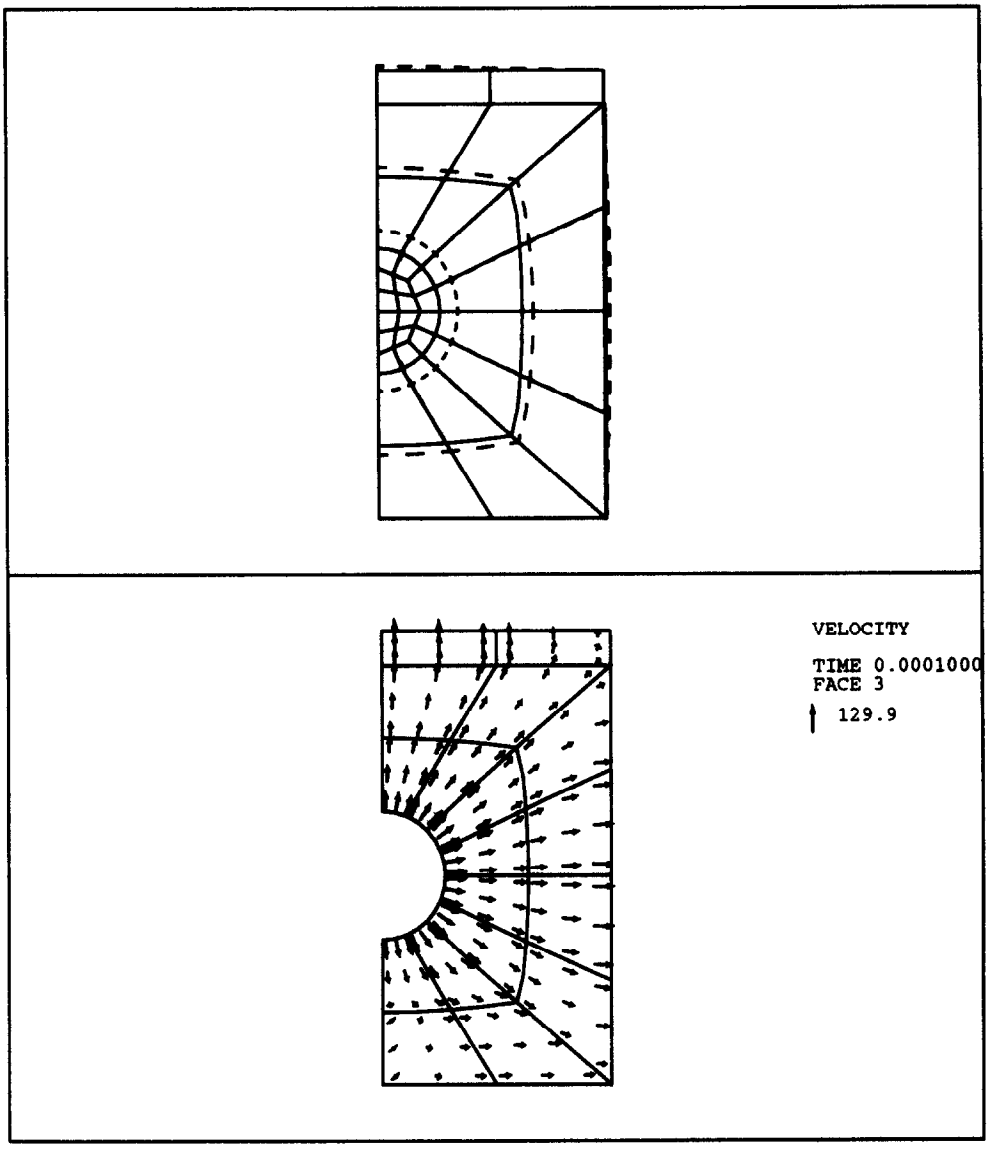

Fig. 22. Gas bubble expanding in a water tank; mesh configuration and velocity distribution in the water at time 1×10^{-4} sec.

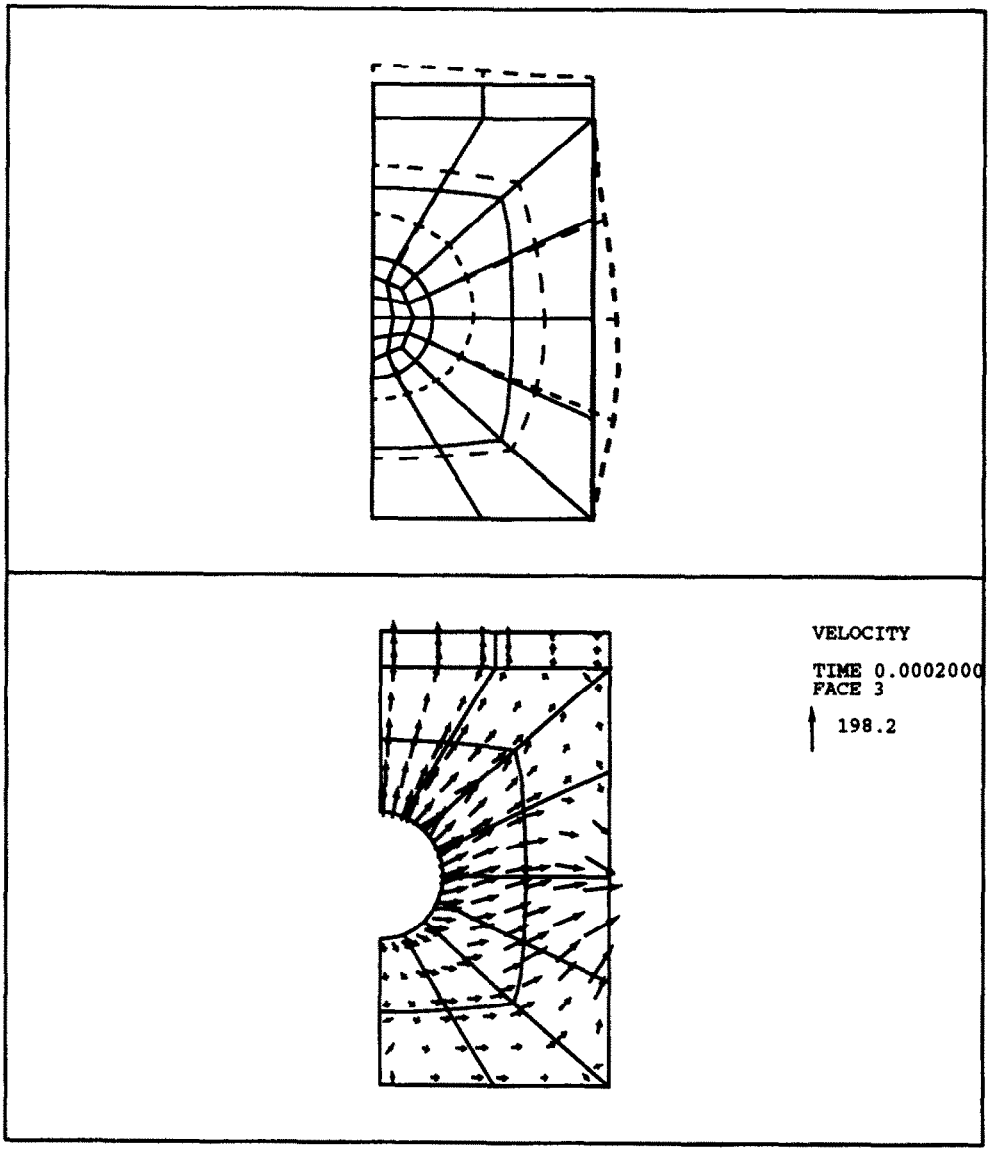

Fig. 23. Gas bubble expanding in a water tank; mesh configuration and velocity distribution in the water at time 2×10^{-4} sec.

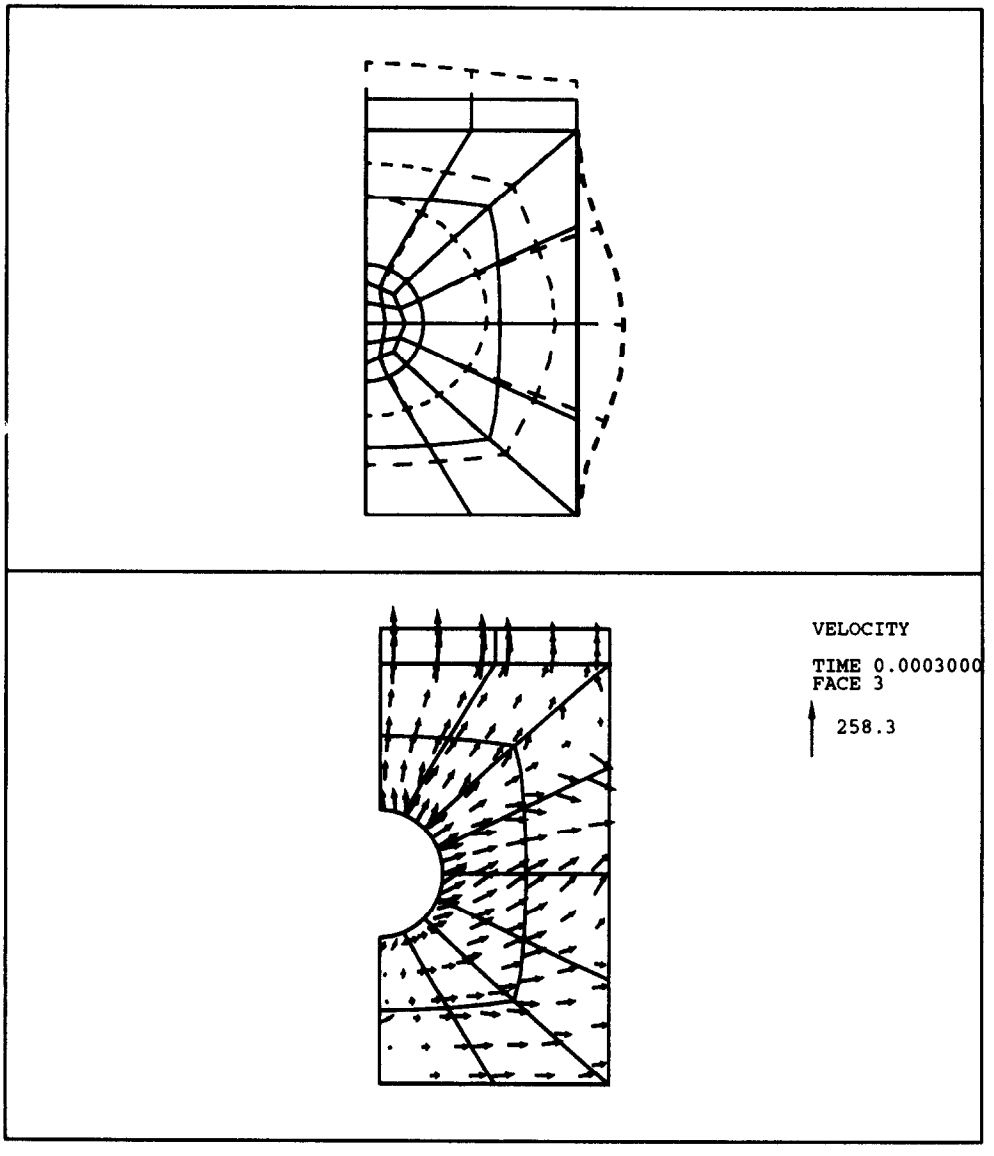

Fig. 24. Gas bubble expanding in a water tank; mesh configuration and velocity distribution in the water at time 3×10^{-4} sec.

Acknowledgements—This research has been supported by the GKSS Forschungsinstitut, Germany, with Mr R. Dietrich the project manager. We gratefully acknowledge this support.

REFERENCES

1. T. B. Belytschko, Methods and programs for analysis of fluid–structure systems. *Nuclear Engng Design* **42**, 41–52 (1977).
2. Y. Hamdi, M. A. an Ousset and G. Verchery, A displacement method for the analysis of vibrations of coupled fluid–structure systems. *Int. J. Numer. Meth. Engng* **13**, 139–150 (1978).
3. L. G. Olson and K. J. Bathe, A study of displacement-based finite elements for calculating frequencies of fluid and fluid–structure systems. *Nuclear Engng Design* **76**, 137–151 (1983).
4. H. C. Chen and R. L. Taylor, Vibration analysis of fluid–solid systems using a finite element displacement formulation. *Int. J. Numer. Meth. Engng* **29**, 683–698 (1990).
5. O. C. Zienkiewicz and P. Bettess, Fluid–structure dynamic interaction and wave forces, an introduction to numerical treatment. *Int. J. Numer. Meth. Engng* **13**, 1–16 (1978).
6. H. Morand and R. Ohayon, Symmetric variational formulations for the elasto-acoustic vibration problem: finite element results. In *Proceedings of the 2nd International Symposium on Finite Element Methods in Flow Problems, ICCAD*, No 2/76. TP-ONERA (1976).
7. H. Morand and R. Ohayon, Substructure variational analysis of the vibrations of coupled fluid structure systems. *Int. J. Numer. Meth. Engng* **14**, 741–755 (1979).
8. G. C. Everstine, A symmetric potential formulation for fluid–structure interaction. *J. Sound Vibr.* **79**, 157–160 (1981).
9. L. G. Olson and K. J. Bathe, Analysis of fluid–structure interactions. A direct symmetric coupled formulation based on the fluid velocity potential. *Comput. Struct.* **21**, 21–32 (1985).

10. E. Kock and L. G. Olson, Fluid–structure interaction analysis by the finite element method—a variational approach. *Int. J. Numer. Meth. Engng* **31**, 463–491 (1991).
11. K. J. Bathe, *Finite Element Procedures in Engineering Analysis*. Prentice-Hall, Englewood Cliffs, NJ (1982).
12. W. F. Noh, CEL: a time-dependent, two-space dimensional, coupled Eulerian–Lagrangian code. In *Methods in Computational Physics* (Edited by B. Alder), p. 117. Academic Press, New York (1964).
13. J. D. Anderson, *Modern Compressible Flow*. McGraw-Hill (1982).
14. T. J. R. Hughes, W. K. Liu and T. K. Zimmermann, Lagrangian–Eulerian finite element formulation for incompressible viscous flows. *Comput. Meth. Appl. Mech. Engng* **29**, 329–349 (1981).
15. A. Huerta and W. K. Liu, Viscous flow with large free surface motion. *Comput. Meth. Appl. Mech. Engng* **69**, 277–324 (1988).
16. K. Muto, Y. Kasai, M. Nakahara and Y. Ishida, Experimental tests on sloshing response of a water pool with submerged blocks. *Proceedings of the 1985 Pressure Vessels and Piping Conference*, Vol. 98-7, *Fluid–Structure Dynamics* (Edited by D. C. Ma and F. J. Moody), pp. 209–214. ASME (1985).